J Geophys (1982) 50:177 – 188

Journal of Geophysics

Numerical Simulation of Vertical Seismic Profiling

P. Temme and G. Müller

Institute of Meteorology and Geophysics, Feldbergstr. 47, 6000 Frankfurt, Federal Republic of Germany

Abstract. Methods for the calculation of synthetic seismograms along vertical profiles through horizontally layered media are presented; the aim is to simulate numerically the technique of vertical seismic profiling (VSP), which is sometimes used for improved resolution of deep primary reflections. We present the theory for vertically travelling plane waves and for spherical waves, generated by a single force or an explosive point source. The solution is restricted to the acoustic case. The theoretical seismograms are complete, i.e., they contain all surface and internal multiples. Anelastic effects are taken into account with the method of complex velocities. In order to save computing time, seismogram segments are calculated, using the method of complex frequencies.

These methods are applied to a layered model of the coal-bearing carboniferous in the Ruhr district of W. Germany. Different assumptions on overburden structure, recording geometry and anelasticity are made, and the VSP seismograms are compared with seismograms calculated for horizontal profiles at the surface. It is suggested that VSP field surveys be preceeded by similar numerical studies for an estimate of the information that can be obtained by this expensive technique.

Key words: Synthetic seismograms — Vertical seismic profiling – Coal prospecting

Introduction

Overburden layers like those in the Ruhr district of the Federal Republic of Germany, have a great influence on seismic prospecting of coal-seam sequences. In the usual line or areal seismic surveys, made at the surface, multiples within the overburden and conversion phases may mask primary reflections from the coal bearing carboniferous, strong frequency dependent absorption changes the excitation signal and the frequency content of reflected waves, passing through the top layers and scattering at inhomogeneities close to the surface results in a reduced signal-to-noise ratio.

These problems, of course, are not restricted to seismic prospecting for coal. A possible reduction of the disturbing influence of the overburden can be obtained by applying vertical seismic profiling (VSP), where receivers are arranged vertically in boreholes. Wuenschel (1976) and Kennett et al. (1980) describe several advantages of this recording geometry, including improvement of signal-to-noise ratio, higher bandwidth, especially better recording of high frequencies, better identification of primary and multiple reflections due to separation of up- and downgoing waves, determination of deconvolution operators from the direct downward travelling wave, better knowledge of the absorption properties of the overburden.

Because VSP is an especially expensive technique, it is desirable to perform numerical simulations of this method prior to the measurements, using all information on the reflecting structure that is already available. Numerical simulation means the calculation of synthetic seismograms for receivers on profiles extending vertically through a layered model of the ground from the surface to arbitrary depth. The synthetic seismograms should be realistic, i.e., they should include all internal and surface multiples, complicated layering should be tractable, and the field geometry and absorption of seismic energy in the layers should be taken into account. Under these circumstances the numerical simulation of VSP may make a valuable contribution to the design of field experiments. The purpose of this paper is to present the theoretical background for the calculation of synthetic VSP seismograms and to illustrate their potential by examples for a model which is typical of the layering in the Ruhr district.

The theoretical approach presented here is restricted to the acoustic case. We present the theory for vertically propagating plane waves and for spherical waves in some detail, since we believe that these methods deserve wider distribution among interpreters and researchers in reflection seismics, at least the methods for the acoustic case, where really complicated layering with arbitrary elastic and anelastic properties can be treated at reasonable computational cost. Of course, the limitation to the acoustic case yields only an approximation of the true elastic wavefield, especially at larger horizontal distances between source and receivers, and Kennett (1979) has emphasized this point. However, Kennett's seismogram calculations for both the acoustic and the elastic case (which includes $P-SV$ interaction) illustrate, in our opinion, that from a practical point of view, the acoustic approximation is often sufficient. The theory, which is presented here with mainly the modelling of vertical seismic profiles in mind, can also be applied to horizontal profiles; the differences between the corresponding computer programs are small.

In the following we start with the theory for vertical plane-wave propagation in a layered half space. Very recently, papers on this special subject have appeared (Wyatt 1981; Ganley 1981), and our method is, in fact, similar to that used by Ganley; we therefore present only a compact outline. We

0340-062X/82/0050/0177/$02.40

then show how calculated plane-wave seismograms can subsequently be corrected for spherical divergence in order to get an approximation of point-source excitation. Exact theoretical seismograms for explosive point sources as well as for vertical single forces at the surface can be obtained from the theory developed in the appendix. A few remarks are added on the implementation of absorption effects by using complex velocities and on the calculation of seismogram segments with the method of complex frequencies, a method by which aliasing in the time domain may be suppressed. Synthetic VSP seismogram sections are then presented for a model of the carboniferous, typical of the Ruhr district, overlain by two different tertiary overburden structures. Different assumptions on the recording geometry and Q structure of the models are made. We finally compare the synthetic VSP sections with horizontal profile sections which simulate the usual line-survey technique at the surface.

Theory

Synthetic Seismograms for Plane-Wave Excitation

We assume a model of $n-1$ layers on top of a half space, which is layer n (Fig. 1). Each layer is described by its parameters d_i = thickness, $\alpha_i = P$-wave velocity, ρ_i = density, and Q_i = quality factor. At the free surface $z_1 = 0$ a seismic source, exciting vertically travelling plane waves, is located. We describe the incident wave by its potential $\phi_0(z,t)$

$$\phi_0(z,t) = F\left(t - \frac{z}{\alpha_1}\right).$$

For many purposes it is easier to work in the frequency domain. The Fourier transform of ϕ_0 is given by

$$\bar{\phi}_0(z,\omega) = \bar{F}(\omega)\, e^{-j\omega\frac{z}{\alpha_1}},$$

where $\bar{F}(\omega)$ is the Fourier transform of the excitation function $F(t)$. For the potential $\bar{\phi}_i(z,t)$ in layer i we assume similarly

$$\bar{\phi}_i(z,\omega) = \bar{F}(\omega)\{A_i e^{-j\omega\frac{z-z_i}{\alpha_i}} + B_i e^{+j\omega\frac{z-z_i}{\alpha_i}}\} \tag{1}$$

with so far unknown coefficients A_i and B_i. Downward travelling waves are represented by the first term of (1), upward travelling waves by the second. The amplitude coefficients A_i and B_i are calculated from the boundary conditions at the interfaces (continuity of vertical displacement $\partial\phi/\partial z$ and normal stress $\rho\partial^2\phi/\partial t^2$):

$$\bar{\phi}'_1 = 0 \quad \text{(free surface at } z = z_1\text{)}. \tag{2}$$

$$\frac{\partial\bar{\phi}_i}{\partial z} = \frac{\partial\bar{\phi}_{i-1}}{\partial z}$$
$$\rho_i\bar{\phi}_i = \rho_{i-1}\bar{\phi}_{i-1} \qquad (\text{at } z = z_i \ (i = 2, 3, \ldots, n)) \tag{3}$$

$\bar{\phi}'_1 = \bar{\phi}_1 - \bar{\phi}_0$ in Eq. (2) represents the potential of all upgoing and downgoing waves in layer 1 except for the incident wave $\bar{\phi}_0$. If we assume an incident wave of unit amplitude, Eq. (2) results in

$$A_1 = 1 - B_1.$$

Equations (3) give for A_i, B_i in layer $i > 1$ the matrix relation

$$\begin{pmatrix} A_i \\ B_i \end{pmatrix} = m_i \begin{pmatrix} A_{i-1} \\ B_{i-1} \end{pmatrix} \tag{4}$$

with the 2×2 layer matrix

$$m_i = \frac{e^{j\omega d_{i-1}/\alpha_{i-1}}}{2\rho_i/\alpha_i} \cdot \begin{pmatrix} (\rho_i/\alpha_{i-1} + \rho_{i-1}/\alpha_i)\, e^{-2j\omega d_{i-1}/\alpha_{i-1}} & (-\rho_i/\alpha_{i-1} + \rho_{i-1}/\alpha_i) \\ (-\rho_i/\alpha_{i-1} + \rho_{i-1}/\alpha_i)\, e^{-2j\omega d_{i-1}/\alpha_{i-1}} & (\rho_i/\alpha_{i-1} + \rho_{i-1}/\alpha_i) \end{pmatrix}. \tag{5}$$

Successive applications of Eq. (4) and additional use of the relation $B_n = 0$, which means that there are no upgoing waves in the halfspace (index n), yields

$$\begin{pmatrix} A_n \\ 0 \end{pmatrix} = M \begin{pmatrix} A_1 \\ B_1 \end{pmatrix} = M \begin{pmatrix} 1 - B_1 \\ B_1 \end{pmatrix} \tag{6}$$

with the layer matrix product

$$M = \begin{pmatrix} M_{11} & M_{12} \\ M_{21} & M_{22} \end{pmatrix} = m_n \cdot m_{n-1} \cdot \ldots \cdot m_2.$$

Solution of Eq. (6) yields

$$B_1 = \frac{M_{21}}{M_{21} - M_{22}} = \frac{R}{1+R}$$

and (7)

$$A_1 = 1 - B_1 = \frac{1}{1+R},$$

where we have introduced the reflectivity $R = -M_{21}/M_{22}$ of the layer stack below $z = z_2$. As shown in the appendix, the reflectivity R can also be calculated by a recursive procedure; this calculation is faster than the calculation via the matrix M.

The amplitude coefficients for $i = 2, 3, \ldots, n$ are determined by the matrix relation

$$\begin{pmatrix} A_i \\ B_i \end{pmatrix} = M_i \begin{pmatrix} A_1 \\ B_1 \end{pmatrix} = M_i \begin{pmatrix} 1 - B_1 \\ B_1 \end{pmatrix}, \tag{8}$$

where the layer matrix product M_i only has to be taken down to layer i:

$$M_i = \begin{pmatrix} M_{i11} & M_{i12} \\ M_{i21} & M_{i22} \end{pmatrix} = m_i \cdot m_{i-1} \cdot \ldots \cdot m_2.$$

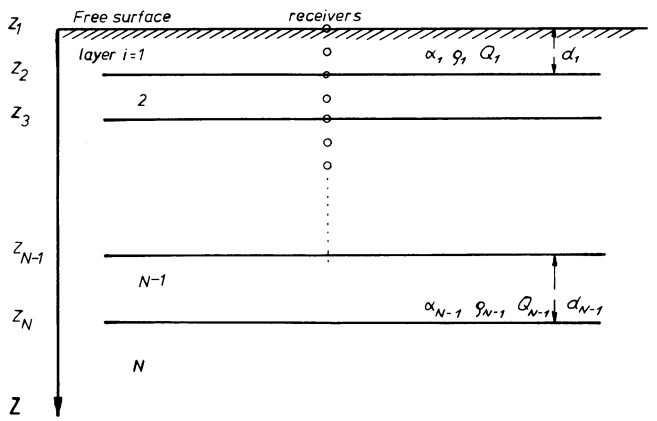

Fig. 1. The general model for computing synthetic seismograms. *Circles* indicate receiver positions. The parameters of layer i are: $\alpha_i - P$ velocity, ρ_i density, Q_i quality factor, d_i layer thickness. z_i $(i = 1, 2, \ldots, n)$ is the depth of interface i

From Eqs. (7) and (8) we obtain:

$$A_i=\frac{M_{i11}+RM_{i12}}{1+R}$$
$$B_i=\frac{M_{i21}+RM_{i22}}{1+R}. \tag{9}$$

Finally, in order to obtain the displacement spectrum, we have to take the derivative of the potential $\bar{\phi}_i$ in Eq. (1) with respect to z. After inverse Fourier transform we find the displacement in layer i,

$$u_i(z,t)=\frac{1}{2\pi}\frac{\alpha_1}{\alpha_i}$$
$$\cdot\int_{-\infty}^{+\infty}\bar{G}(\omega)\{A_i e^{-j\omega\frac{z-z_i}{\alpha_i}}-B_i e^{+j\omega\frac{z-z_i}{\alpha_i}}\}\,e^{j\omega t}\,d\omega, \tag{10}$$

where $\bar{G}(\omega)=-\bar{F}(\omega)\frac{j\omega}{\alpha_1}$ is the spectrum of the displacement of the incident wave at $z_1=0$.

Equation (10) allows fast wavefield calculations for arbitrary receiver depth in the layered medium. The seismograms are complete, i.e., all internal and surface multiples are included.

Synthetic Seismograms for Point-Source Excitation

In realistic field experiments point sources which generate spherical waves are used. Thus amplitudes of reflected waves are not only affected by reflection coefficients and absorption, but also by spherical divergence. In the appendix the theory of point source excitation dealing with the explosive and vertical single force case is presented. In principle the Sommerfeld integral is used to decompose the direct spherical wave into plane waves, and the corresponding plane wave responses of the medium are superposed to give the spherical-wave response. Because typically several hundred plane-wave cases have to be solved, the computing time is much longer than that needed for the evaluation of Eq. (10).

In the following we present an approximation of the spherical-wave case, which can easily be applied to seismograms calculated from the plane-wave theory. Thus we can simulate VSP in the special case where receivers are buried *vertically beneath the point source*. The method has been described by Müller (1971) for receivers at the surface; the plane-wave seismogram at the arrival times of primary reflections is multiplied by the divergence factors of these reflections and by interpolated values in between. Suppose now, a receiver is buried at depth z in layer i. Thus, the primary reflection from interface k ($k=i+1, i+2, \ldots, n$) has the travel-time

$$t_k=\sum_{j=1}^{k-1}\frac{2d_j}{\alpha_j}-\sum_{j=1}^{i-1}\frac{d_j}{\alpha_j}-\frac{z-z_i}{\alpha_i}.$$

The divergence factor by which the plane-wave seismogram is multiplied at this time is

$$G_k=\frac{\alpha_1}{\sum_{j=1}^{k-1}2d_j\alpha_j-\sum_{j=1}^{i-1}d_j\alpha_j-(z-z_i)\alpha_i}.$$

In the case of receivers at depth, the direct wave has to be corrected accordingly:

$$t_1=\sum_{j=1}^{i-1}\frac{d_j}{\alpha_j}+\frac{z-z_i}{\alpha_i},$$
$$G_1=\frac{\alpha_1}{\sum_{j=1}^{i-1}d_j\alpha_j+(z-z_i)\alpha_i}.$$

Between the times t_1, t_{i+1}, t_{i+2}, ..., t_n we apply a linear interpolation, and for $t>t_n$ the seismogram is damped according to $G=G_n\cdot t_n/t$. The direct wave and primary reflections are corrected exactly by this procedure; it turns out that multiple reflections are suppressed too much. However, the comparison with seismograms calculated by the exact spherical theory shows that this simple method often is an acceptable approximation.

Causal Absorption

When synthetic seismograms are used to simulate wave propagation in realistic media, the computational methods should take account of absorption, particularly at the high frequencies used in coal-seam prospecting where absorption strongly influences the waves. Anelasticity can be incorporated into the methods described in this paper by making the wave velocities complex. Like O'Neill and Hill (1979) we use the following complex velocity law:

$$\alpha(\omega)=\alpha_r\left(1+\frac{1}{\pi Q}\ln\frac{\omega}{\omega_r}+\frac{j}{2Q}\right). \tag{11}$$

Here Q is the quality factor, assumed to be frequency independent, ω_r is a reference frequency and α_r is the (real) velocity at the reference frequency, assumed to be known. In calculations for seismic prospecting one would choose $f_r=\omega_r/2\pi$ roughly around 100 Hz. The velocity law (11) corresponds to causal absorption and hence implies a slight velocity dispersion.

Aliasing in the Time Domain

In numerical calculations of theoretical seismograms the seismogram length strongly influences the computimg time, since usually the spectra are calculated for equidistant frequencies and the frequency interval is the reciprocal value of this length. For complicated models, especially those having a free surface, the duration of the complete seismogram can be very long, and the number of frequencies in a specified frequency window is proportional to duration. If we choose a time window shorter than the response of the medium in order to save computing time, those parts of the response beyond the end of the seismogram will not be suppressed, but appear in the early parts of the seismogram and interfere with early arrivals. This situation is completely analogous to aliasing in the frequency domain and therefore is called aliasing in the time domain.

An effective method to avoid or reduce aliasing in the time domain has been in use in seismology for quite some time (Rosenbaum 1974; Bouchon 1979). The basic idea is to calculate first the *damped* seismogram $u_\tau(t)=u(t)e^{-t/\tau}$ instead of $u(t)$ by evaluating the Fourier transform $\bar{u}(\omega)$ of $u(t)$ at complex frequencies $\omega-j/\tau$ and using the damping theorem of Fourier transforms: $\bar{u}_\tau(\omega)=\bar{u}(\omega-j/\tau)$. Evidently, $u_\tau(t)$ is less disturbed by aliasing than $u(t)$. Multiplication of $u_\tau(t)$ by $e^{+t/\tau}$ in a second step gives the desired seismogram $u(t)$. Experiments with this method, with τ equal 20–40% of the desired length of $u(t)$, show good results.

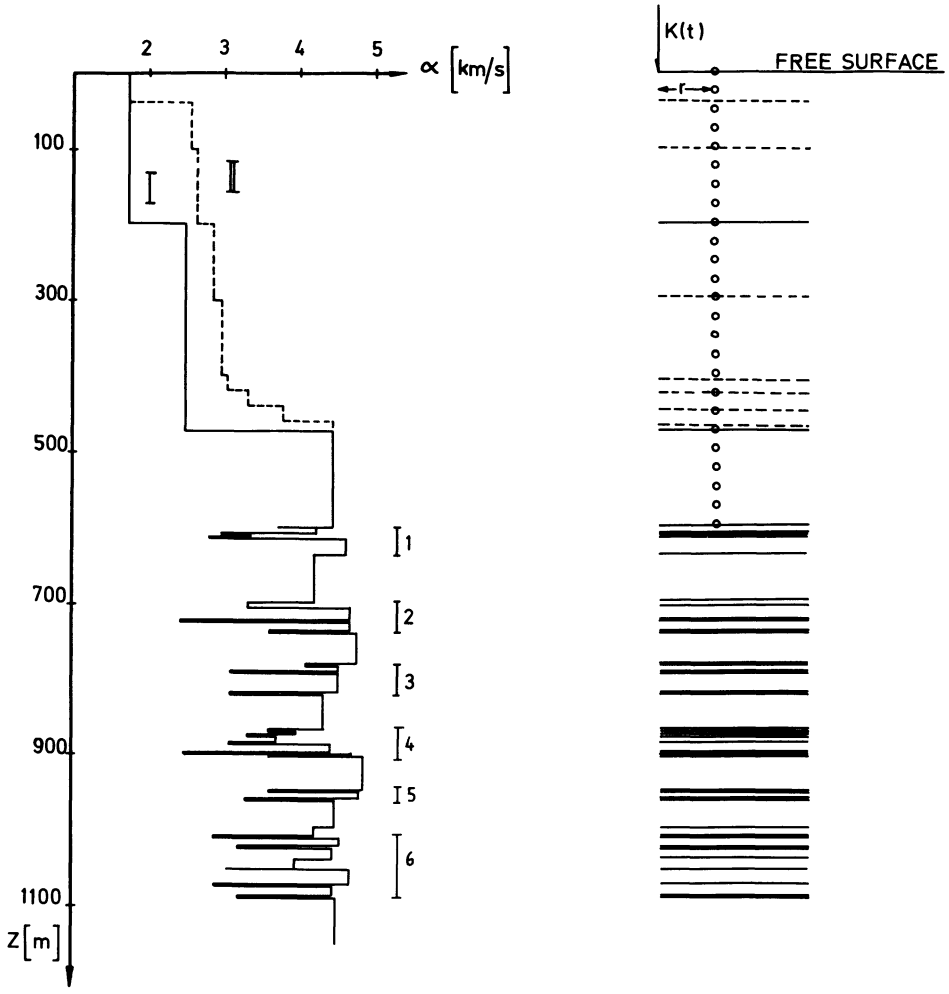

Fig. 2. *Left:* A typical velocity-depth model from the Ruhr district, W. Germany. The carboniferous is subdivided into 6 seam groups, indicated by *vertical bars* and combined with two different overburden models, a simple 3-layer overburden (model I) and a complicated 9-layer overburden (model II, *dashed line*)
Right: Corresponding layer sequences; *circles* indicate vertical seismic profile. $K(t)$, single force; r, offset from source to receiver array

Synthetic Seismograms

In the following we present synthetic seismograms, calculated for the complicated layering shown in Figure 2. A continuous borehole profile from the Ruhr district in W. Germany was approximated by a discretized velocity-depth function, where the coal-seam sequence extends in the depth range 600–1100 m, showing strong velocity inversions with a maximum reflection coefficient of 0.4 at depth 900 m. The density of each layer was calculated from the relation $\rho = 1.7 + 0.2\alpha$. We subdivided the seam sequence into 6 seam groups, denoted by vertical bars. The carboniferous was combined with two different types of overburden structure. Model I in Fig. 2 has a simple 3-layer overburden with strong reflection coefficients, whereas in model II there is a more gradual transition from the surface to the carboniferous, consisting of 9 layers. The receivers are arranged on a vertical array extending from the surface to the level 600 m, with a depth interval of 25 m. A seismic source, exciting vertically travelling plane waves or spherical waves, is located at the free surface. In the spherical-wave case the source is a vertical single force, and the receivers may have an arbitrary offset r.

Model I

Figure 3 shows the calculated VSP seismograms for plane-wave excitation with a dominant frequency of 100 Hz in the case of relatively weak absorption ($Q = 1000$ in all layers). In order to save computing time, the response, which has a duration of nearly 8 s, is only calculated for a time segment of 1 s using the method of complex frequencies described above; it took a computing time of about 2.5 min on a DEC1091 to calculate this section. Downgoing waves with positive velocities are clearly separated in Fig. 3 from upcoming waves with negative velocities. The first arrival in each seismogram is the direct, downward travelling wave. The interfaces of the 3-layer overburden can be identified at the depths z_2 and z_3, where the direct wave coincides with primary reflections from the overburden. At the surface the amplitudes of reflections are doubled. From there the upcoming waves are reflected back as surface multiples into the structure. Within each layer, the amplitudes remain constant, as we expect for plane waves in elastic media. At interfaces the transmitted waves are affected only by the transmission coefficient, primary reflections from the seam groups, indicated by bars in Fig. 2, are affected only by the transmission coefficient. Primary reflections from the groups 1, 2 and 3 can be identified clearly. Each reflection is a complicated interference signal. The deepest traces, in the depth range 425–600 m, contain seam-group reflections, which are undisturbed by overburden multiples.

Figure 4 demonstrates the influence of the frequency content of the excitation signal. We have now assumed a dominant frequency of 50 Hz; all other parameters are the same as in the calculation for Fig. 3. This seismic section shows

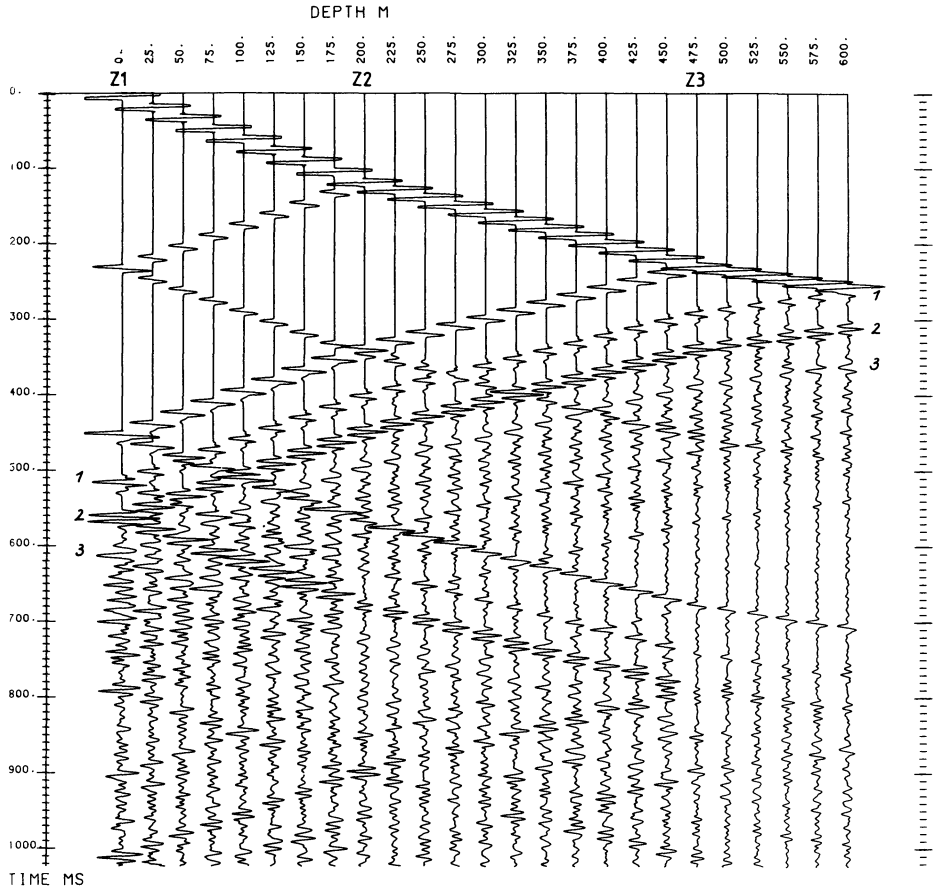

Fig. 3. VSP section for model I and plane-wave excitation with a dominant frequency of 100 Hz; seismograms are normalized to the maximum of the deepest trace. z_1, z_2 and z_3 indicate overburden interfaces. Seam-group reflections are indicated by *1*, *2*, *3*

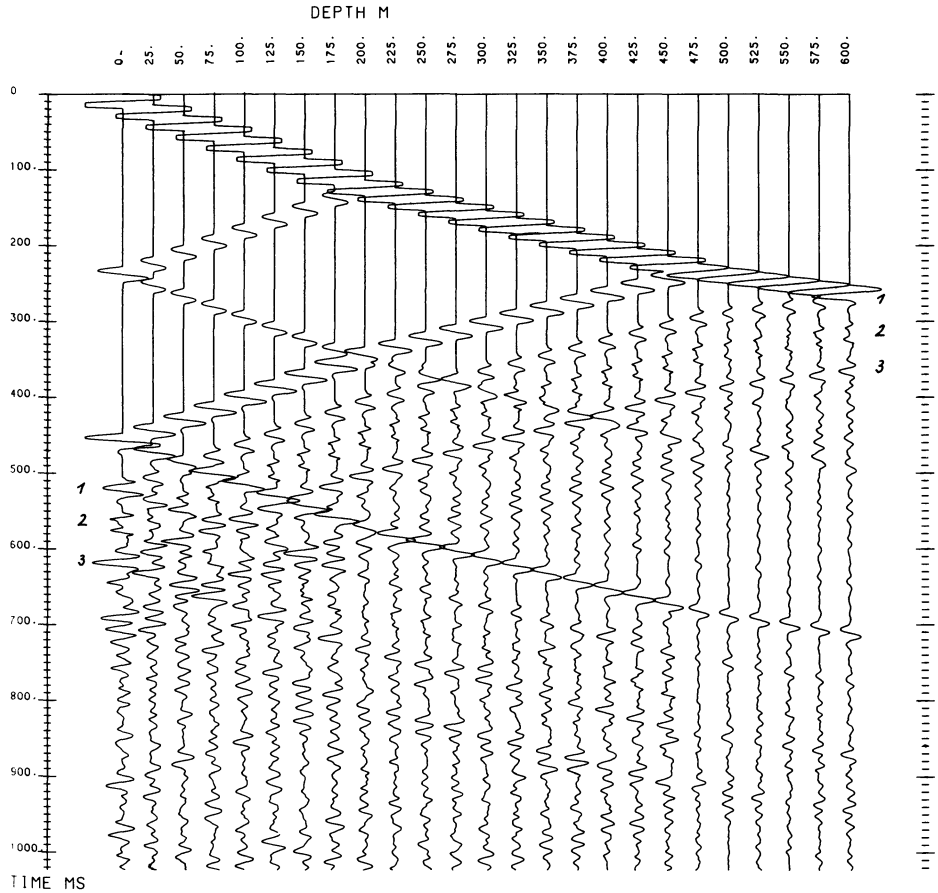

Fig. 4. VSP section for model I and plane-wave excitation with a dominant frequency of 50 Hz

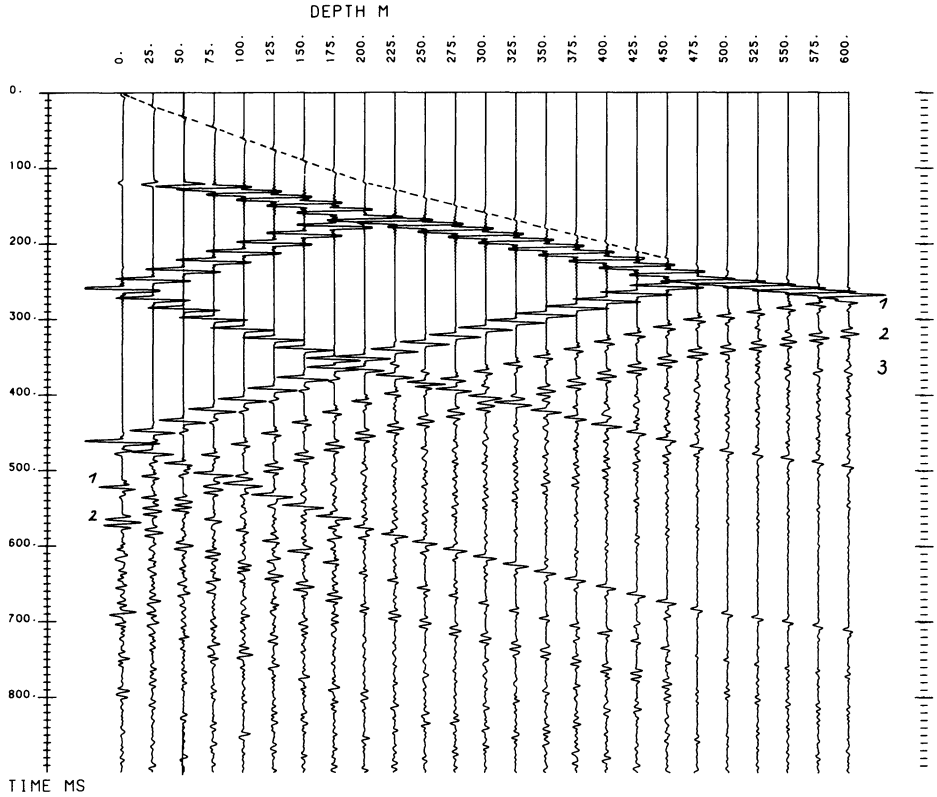

Fig. 5. VSP section for model I and spherical-wave excitation at the surface; offset $r = 200$ m. The *dashed line* indicates a numerical phase without physical significance. Seam-group reflections are indicated by *1, 2, 3*

strongly modified primary reflections from the seam groups. The amplitude ratio between them is changed, particularly in that the reflection from seam group 2 becomes much weaker relative to the reflections 1 and 3. Thus, a shift in dominant frequency of seismic waves used for coal prospecting may strongly enhance or reduce a particular seam-group reflection. Broadband recording and subsequent bandpass filtering in different frequency bands may therefore be quite helpful for the identification of seam groups.

If we use a vertical single force at the free surface, which excites spherical waves with again 100 Hz dominant frequency, we obtain the VSP synthetic seismograms in Fig. 5, calculated for an offset of $r = 200$ m. Compared to the plane-wave case in Fig. 3 the traveltime curves of all phases are now curved, and the amplitudes of up- and downgoing waves are no longer constant within the layers. Relative to the direct wave, the primary reflections from the seam groups become weaker. Only seam groups 1 and 2 can be identified clearly and show nearly the same interference signals as in Fig. 3; the seam group reflection 3 is much weaker. The computing time to calculate this section was about 2 h.

The theory of spherical waves allows also the calculation of synthetic seismograms on a horizontal profile. For receivers located on a line extending from 100–1100 m, we obtain the section shown in Fig. 6. The first arrival D is the strongly attenuated direct wave which travels along the top of the first layer. The primary reflection R_1 from the first overburden interface arrives at 230 ms. Beyond the critical distance of about 600 m, we then record the refracted wave from the second layer as a first arrival. At 440 ms the second primary reflection R_2 from depth level 475 m arrives, followed immediately by a multiple reflection of R_1. Within the time window of 500 ms to 650 ms, we can identify the primary reflections from the seam groups 2 and 3. Beyond a distance of 500 m they interfere strongly with multiples and primary reflections from the overburden. Compared to the VSP seismograms in Figs. 3 and 5, multiple events cannot easily be separated from primary reflections of the seam groups.

Model II

In order to study the influence of multiple reflections and adsorption in the overburden, VSP seismograms for a more complicated layering (model II) were calculated. Figure 7 shows the synthetic section for $Q = 1000$ everywhere and for spherical-wave simulation, as described above. The direct wave D is followed by a strong multiple M of the reflection from the first overburden interface at depth 35 m. The primary reflections from the seam groups 1, 2 and 3 stand out clearly, but they begin to interfere with the multiple reflection M in the depth range below 500 m. As already mentioned, the spherical-wave approximation corrects exactly the primary reflections only, but attenuates multiple reflections too much. Thus, one could expect a small influence of multiples on seam reflections in the depth range 150–400 m.

If we want to model strong anelastic effects in the overburden by assuming $Q = 100$, we obtain the section shown in Fig. 8. The amplitudes of the seismograms are now normalized with respect to the maximum of the seismogram at the depth 600 m in Fig. 7; thus seismograms of Figs. 7 and 8 are directly comparable. Wave amplitudes are strongly attenuated due to anelastic effects, and the accompanying dispersion can be seen. Primary reflections from the seam groups are clearly visible in the depth range 300–600 m only. The disturbing influence of overburden multiples on primary reflections from the seam sequence is reduced.

Figure 9 shows the synthetic seismograms for the exact spherical-wave case; they were calculated for an offset of $r = 200$ m and $Q = 1000$ throughout model II. A weak, non-

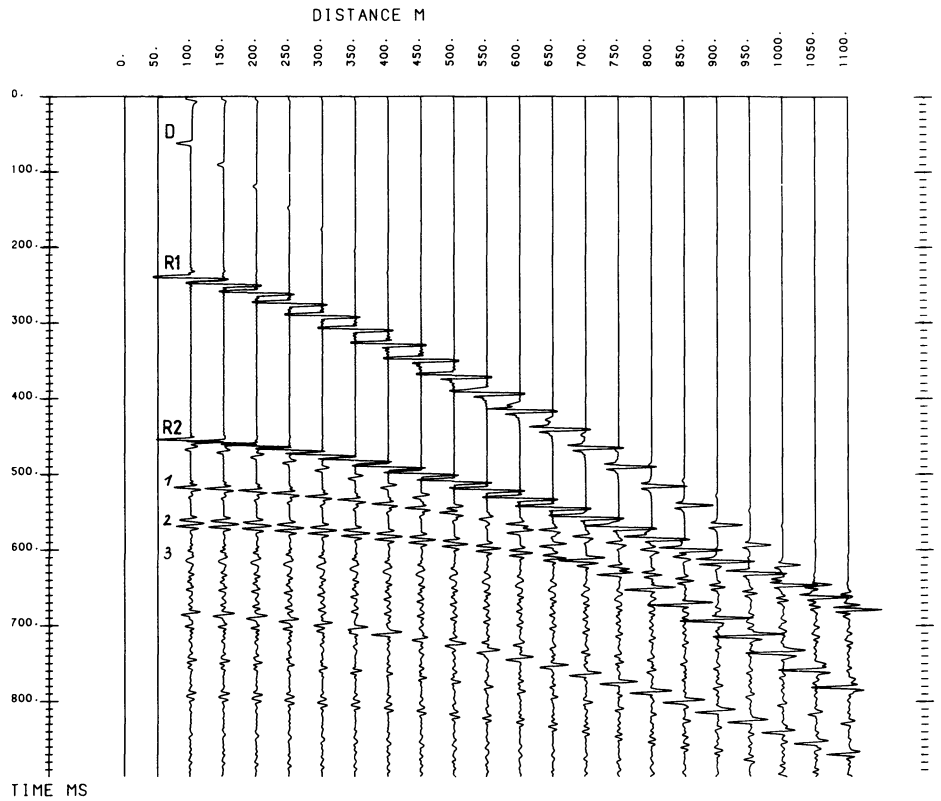

Fig. 6. Horizontal-profile section for spherical-wave excitation at the surface of model I, seismograms are normalized to the maximum of the most distant trace. *D*, direct wave; *R*1, reflection from the first overburden interface; *R*2, reflection from the second overburden interface. Seam-group reflections indicated by *1*, *2*, *3*

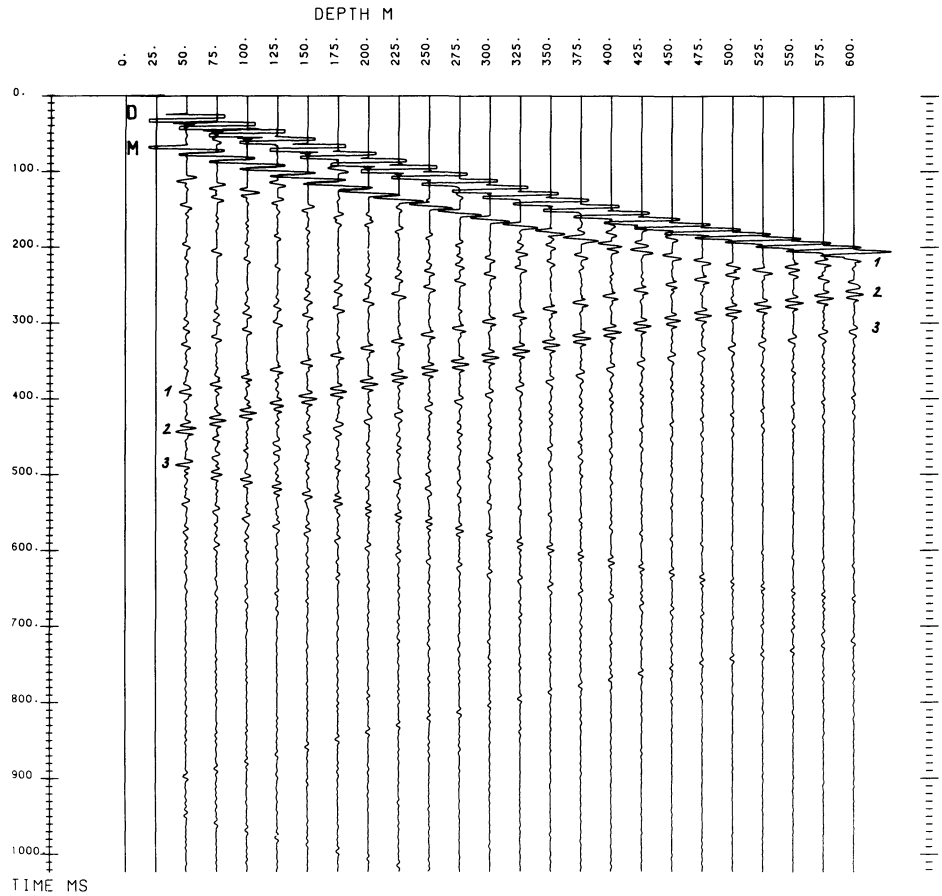

Fig. 7. VSP section for model II and spherical-wave simulation with offset $r=0$; $Q=1000$ everywhere. *D*, direct wave; *M*, surface multiple from the first overburden interface. Traces at 0 and 25 m are set zero for plotting reasons

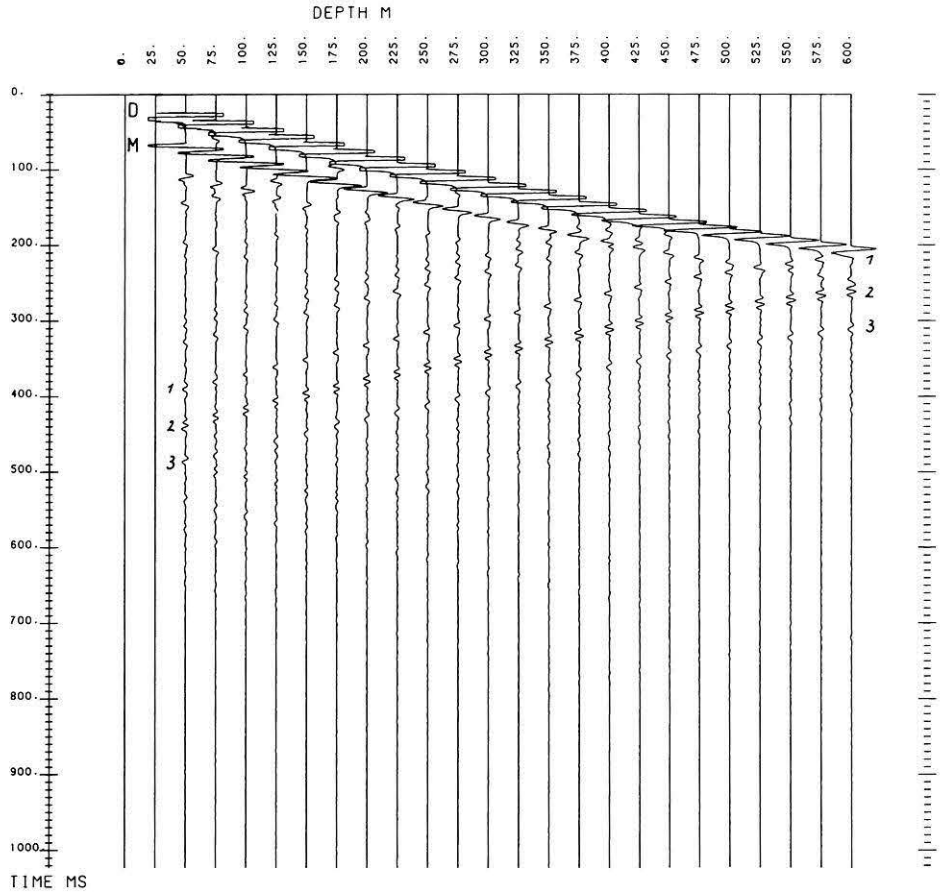

Fig. 8. VSP section for model II and spherical-wave simulation with offset $r = 0$; $Q = 100$ throughout the overburden and $Q = 1000$ elsewhere. Section is normalized with respect to the maximum of the deepest trace in Fig. 7

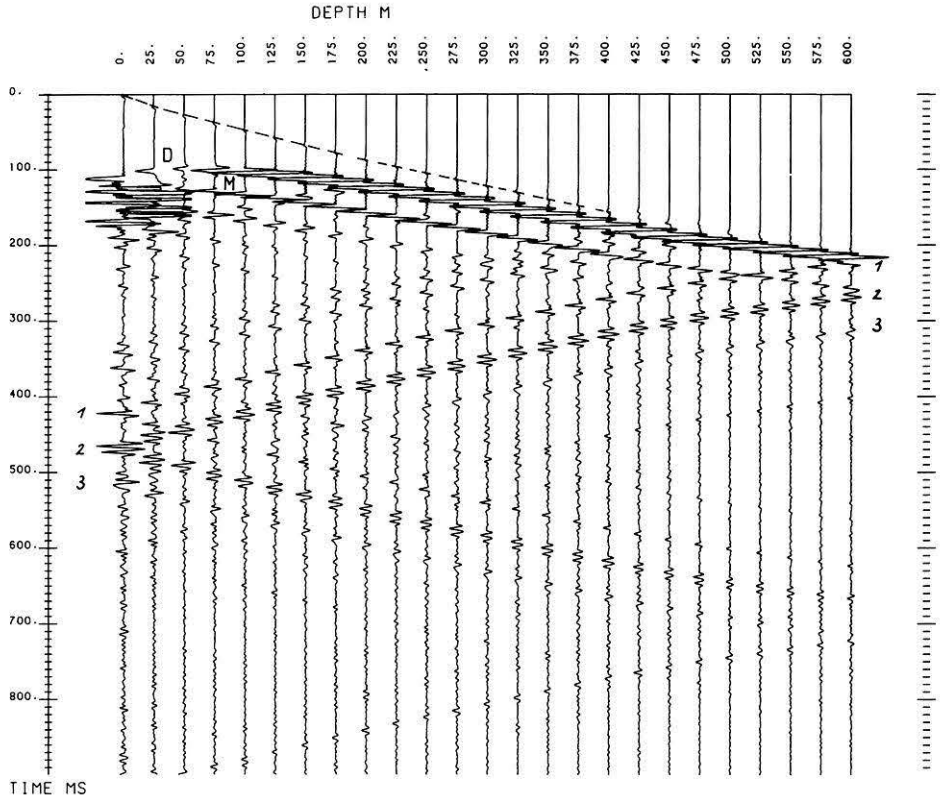

Fig. 9. VSP section for model II and spherical-wave excitation by a single force at the surface; offset $r = 200$ m, D, direct wave; M, surface multiple from the first overburden interface. The *dashed line* indicates a numerical phase

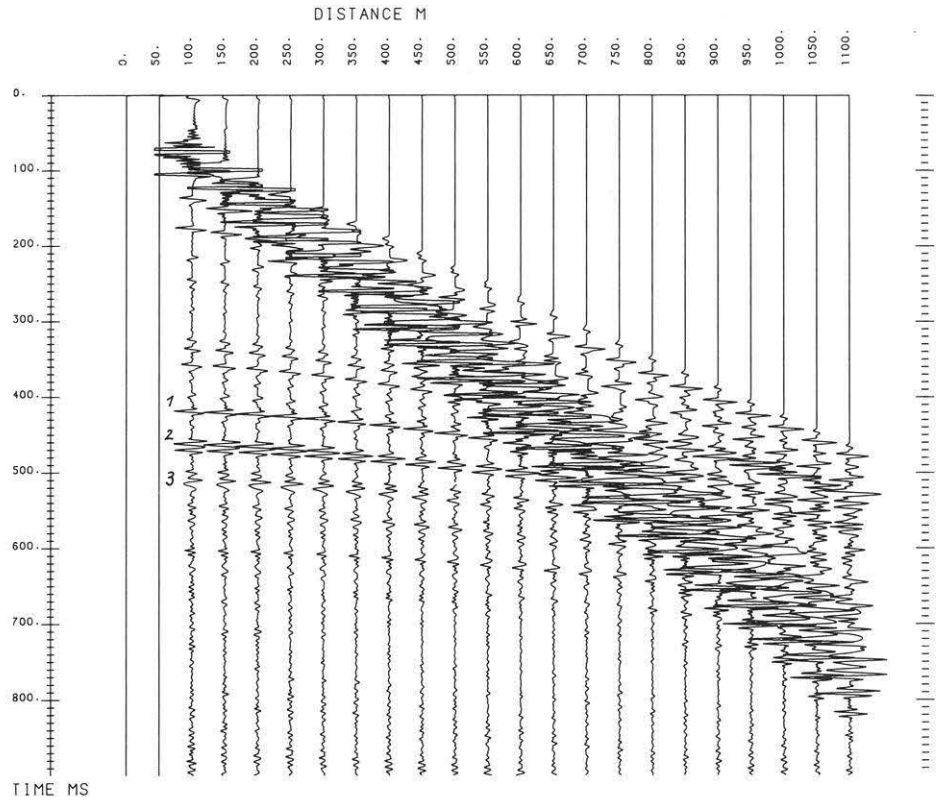

Fig. 10. Horizontal-profile section at the surface of model II for spherical-wave excitation (single force). Seismograms are normalized with respect to the maximum of the most distant trace

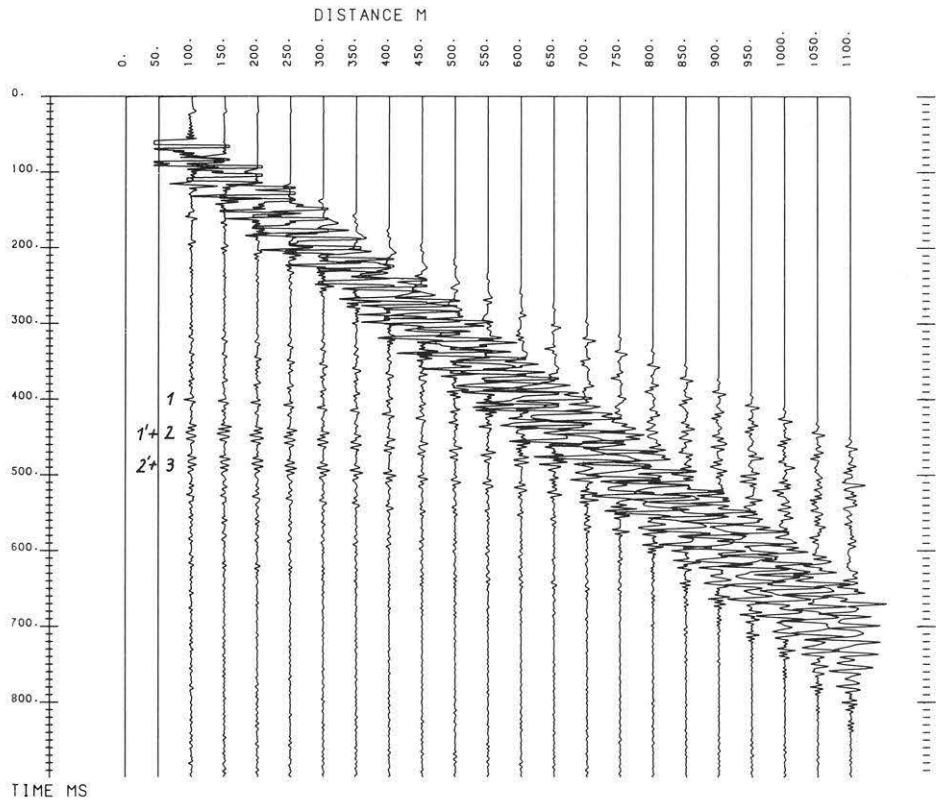

Fig. 11. Horizontal-profile section at the surface of model II for spherical-wave excitation (explosion source at depth 30 m). Seismograms are normalized with respect to the maximum of the most distant trace. The main band of energy in this section is stronger than in the section of Fig. 10 because horizontal radiation is stronger for an explosion than for a vertical single force. Seam-group reflections *1'* and *2'* are due to the ghost reflection at the source

disturbing numerical arrival is followed by the direct downgoing wave *D*; the first arrival at the depths 0 and 25 m is the refracted wave from the first overburden interface. Within the first layer supercritical reflections produce strong amplitudes in the time interval 100–200 ms. Many features in Fig. 9 are quite similar to those in Fig. 7, except that multiple phases (which are correctly modelled in Fig. 9) are considerably stronger.

The synthetic seismogram section for a horizontal profile at the surface of model II is shown in Fig. 10; the correspond-

ing section for model I was given in Fig. 6. Strong amplitudes of multiple reflections in the first layer are visible in the whole distance range from 100–1100 m and cancel primary seam-group reflections beyond a distance of 500 m. Multiple reflections within the whole overburden disturb these reflections at shorter distances more than in the VSP seismograms of Fig. 9. For instance, only a small portion of energy in the wave group 3 in Fig. 10 is really caused by the seam-group reflection 3. Hence, it appears that the disturbing effects of a complicated overburden are more pronounced on horizontal than on vertical seismic profiles.

Our final example of synthetic seismograms (Fig. 11) corresponds to an explosive point source at a depth of 30 m in model II and to a horizontal profile at the surface. Now the surface reflection at the source (ghost reflection) entails doubling of all arrivals in comparison with Fig. 10, such that a really complicated section results. For instance, the seam-group reflections 1′ and 2′, which are a consequence of the ghost reflection, interfere with the direct seam-group reflections 2 and 3, respectively. We mention in passing that the computing time for Fig. 11 was much reduced in comparison with that for Fig. 10, since the reflectivity of model II, of course, had not to be recalculated.

Conclusions

With the method described above it is possible to calculate realistic seismograms on vertical as well as on horizontal seismic profiles through complicated layering at reasonable computational cost. The case of vertical seismic profiling can be modelled very quickly by using simple plane-wave theory and correcting approximately for spherical divergence. In this way the effects due to multiple reflections and absorption can be estimated, and some idea can be obtained about the depths at which receivers should be buried and what frequencies should be used in a field experiment, provided that some information on the structure is available in advance. The more sophisticated spherical wave theory yields additional information on the influence of the offset between source and receiver array. It also allows the simulation of the usual horizontal-profile observations at the surface and thus helps in deciding whether or not the expensive VSP-technique can really be expected to improve the identification of primary and multiple reflections and to reduce significantly the influence of absorption. In the case studied in this paper it appears that this is actually so, but this result cannot be generalized. Hence, a planned field survey should probably be preceeded by numerical studies with the methods developed above.

Acknowledgements. This work was supported financially by Ruhrkohle AG and the government of the state of Nordrhein-Westfalen, Federal Republic of Germany. The computations were performed at the computing center, University of Frankfurt. We are grateful to R. Kind for drawing our attention to the possibility of reducing time-domain aliasing by the use of complex frequencies and for discussions on the subject of this paper. Thanks for discussions go also to J. Fertig. We thank I. Hörnchen for typing the manuscript.

Appendix. *Synthetic Seismograms for Point-Source Excitation*

We treat the case of an explosive point source in the first layer of a horizontally layered medium. This case simulates reasonably well the excitation of seismic waves by explosions and similar sources in reflection measurements on land or sea. For simplicity we consider only acoustic waves. The geometry of the medium is the same as in Fig. 1; the source depth is z_s with $0<z_s<z_2$, and the receiver can be at any depth and horizontal offset. We work with displacement potentials and use cylindrical coordinates (r, φ, z). Because of symmetry reasons there is independence of the azimuth φ; r is the horizontal source-receiver distance.

For the Fourier transformed potential of the direct wave in layer 1 we use the Sommerfeld integral

$$\bar{\phi}_0=\bar{F}(\omega)\int_0^\infty \frac{k}{jl_1}J_0(kr)\,e^{-jl_1|z-z_s|}\,dk, \tag{A-1}$$

where $\bar{F}(\omega)$ is the spectrum of the excitation function, k the horizontal wavenumber, $l_1=(\omega^2/\alpha_1^2-k^2)^{1/2}$ the vertical wavenumber, and $J_0(kr)$ the Bessel function of first kind and order zero.

Similar representations are sought for the potential in an arbitrary layer with index i:

$$\bar{\phi}_i=\bar{F}(\omega)\int_0^\infty \frac{k}{jl_1}J_0(kr)\cdot\{A_i e^{-jl_i(z-z_i)}+B_i e^{+jl_i(z-z_i)}\}\,dk \tag{A-2}$$

$$l_i=(\omega^2/\alpha_i^2-k^2)^{1/2}\qquad (l_i>0 \text{ or } \operatorname{Im} l_i<0).$$

This integral solves the wave equation in layer i. As in the plane-wave case with normal incidence, treated in the main part of the paper, the first term in the curly brackets of (A-2) represents all downgoing waves in layer i and the second term all upgoing waves, and the amplitude coefficients A_i and B_i are calculated from the boundary conditions at the interfaces (continuity of normal displacement and normal stress):

$$\left.\begin{aligned}\frac{\partial\bar{\phi}_i}{\partial z}&=\frac{\partial\bar{\phi}_{i-1}}{\partial z}\\ \rho_i\bar{\phi}_i&=\rho_{i-1}\bar{\phi}_{i-1}\end{aligned}\right\}\quad \text{at}\quad z=z_i\ (i=2,3,\ldots,n) \tag{A-3}$$

$$\bar{\phi}_1=0\qquad\qquad \text{at}\quad z=z_1=0. \tag{A-4}$$

Equation (A-3) yields the matrix relation

$$\begin{pmatrix}A_i\\B_i\end{pmatrix}=m_i\begin{pmatrix}A_{i-1}\\B_{i-1}\end{pmatrix} \tag{A-5}$$

with the 2×2 layer matrix

$$m_i=\frac{e^{+jl_{i-1}d_{i-1}}}{2\rho_i l_i}\begin{pmatrix}(\rho_i l_{i-1}+\rho_{i-1}l_i)e^{-2jl_{i-1}d_{i-1}}(-\rho_i l_{i-1}+\rho_{i-1}l_i)\\(-\rho_i l_{i-1}+\rho_{i-1}l_i)e^{-2jl_{i-1}d_{i-1}}(\rho_i l_{i-1}+\rho_{i-1}l_i)\end{pmatrix}. \tag{A-6}$$

The layer matrix in the main part, Eq. (5), follows from (A-6) for $k=0$.

Layer 1 requires a special treatment, because the source potential $\bar{\phi}_0$ in (A-1) has to be included in $\bar{\phi}_1$. Above the source ($z<z_s$) we use the denotation $\bar{\phi}_1=\bar{\phi}_1^+$ with amplitude coefficients A_1^+ and B_1^+, and below the source ($z>z_s$) we have the quantities $\bar{\phi}_1^-$, A_1^- and B_1^-. The relation between the two pairs of coefficients is

$$\begin{pmatrix}A_1^-\\B_1^-\end{pmatrix}=\begin{pmatrix}A_1^+\\B_1^+\end{pmatrix}+\begin{pmatrix}A_s\\-1/A_s\end{pmatrix},\quad \text{where}\quad A_s=e^{+jl_1z_s}. \tag{A-7}$$

We then apply (A-5) successively, use additionally the relations $B_n=0$ (no upgoing wave in the half-space with index n) and $B_1^+=-A_1^+$ (from boundary condition (A-4)), and introduce (A-7):

$$\begin{pmatrix}A_n\\0\end{pmatrix}=M\begin{pmatrix}A_1^-\\B_1^-\end{pmatrix}=M\begin{pmatrix}A_1^+\\-A_1^+\end{pmatrix}+M\begin{pmatrix}A_s\\-1/A_s\end{pmatrix} \tag{A-8}$$

with the layer-matrix product

$$M=\begin{pmatrix}M_{11}&M_{12}\\M_{21}&M_{21}\end{pmatrix}=m_n\cdot m_{n-1}\cdot\ldots\cdot m_2. \tag{A-9}$$

The second of the two equations (A-8) can be solved for A_1^+:

$$A_1^+ = \frac{M_{21}A_s - M_{22}/A_s}{M_{22} - M_{21}}, \quad B_1^+ = -A_1^+. \tag{A-10}$$

Introducing these results into (A-7) yields:

$$A_1^- = \frac{M_{22}}{M_{22} - M_{21}}(A_s - 1/A_s), \quad B_1^- = RA_1^-. \tag{A-11}$$

The amplitude coefficients for $i = 2, 3, \ldots, n$ follow from the matrix relation

$$\begin{pmatrix} A_i \\ B_i \end{pmatrix} = M_i \begin{pmatrix} A_1^- \\ B_1^- \end{pmatrix},$$

where

$$M_i = \begin{pmatrix} M_{i11} & M_{i12} \\ M_{i21} & M_{i22} \end{pmatrix} = m_i \cdot m_{i-1} \cdot \ldots \cdot m_2 \tag{A-12}$$

is the layer-matrix product taken down to layer i. Using (A-11) we have:

$$A_i = \frac{M_{i11}M_{22} - M_{i12}M_{21}}{M_{22} - M_{21}}(A_s - 1/A_s),$$

$$B_i = \frac{M_{i21}M_{22} - M_{i22}M_{21}}{M_{22} - M_{21}}(A_s - 1/A_s). \tag{A-13}$$

A computational advantage, both with respect to accuracy and computing time, is obtained by observing that the only quantity, related to matrix M and needed in (A-10), (A-11) and (A-13), is the plane-wave reflectivity $R = -M_{21}/M_{22}$ of the layer stack below layer 1:

$$A_1^+ = -\frac{RA_s + 1/A_s}{1+R}, \quad B_1^+ = -A_1^+, \tag{A-14}$$

$$A_1^- = \frac{A_s - 1/A_s}{1+R}, \quad B_1^- = RA_1^-, \tag{A-15}$$

$$A_i = \frac{M_{i11} + RM_{i12}}{1+R}(A_s - 1/A_s),$$

$$B_i = \frac{M_{i21} + RM_{i22}}{1+R}(A_s - 1/A_s) \quad (i = 2, 3, \ldots, n). \tag{A-16}$$

The reflectivity R can be computed recursively (Brekhovskikh 1960). For this purpose we define the reflectivity with respect to the depth $z = z_i$ by the ratio $R_i = B_i/A_i$ of the amplitudes of all upgoing and all downgoing waves in layer i. Then we find the relation between R_{i-1} and R_i from (A-5):

$$R_{i-1} = \frac{r_i + R_i}{1 + r_i R_i} e^{-2jl_{i-1}d_{i-1}}$$

$$r_i = \frac{\rho_i l_{i-1} - \rho_{i-1} l_i}{\rho_i l_{i-1} + \rho_{i-1} l_i}$$

$$= \text{plane-wave reflection coefficient of interface } z = z_i. \tag{A-17}$$

The recursion is started with $i = n$, $R_n = 0$, and is stopped at $i = 2$: the result R_1 of the last step in the recursion is the desired reflectivity R. The reflectivity for vertically travelling waves, which is needed in Eqs. (7) and (9) of the main paper, follows from (A-17) by setting $l_k = \omega/\alpha_k$.

Formulas (A-14) to (A-16), together with (A-2) allow wavefield calculations for arbitrary receiver depths and distances from the source in the layered medium. For applications it is better to work in terms of integrals over slowness $u = k/\omega$ rather than integrals over wavenumber k. The vertical wavenumbers transform according to $l_i = \omega q_i$, where $q_i = (\alpha_i^{-2} - u^2)^{1/2}$. The spectra of the horizontal and vertical displacements, $\bar{u}_{ri} = \partial\bar{\phi}_i/\partial r$ and $\bar{u}_{zi} = \partial\bar{\phi}_i/\partial z$, respectively, are:

$$\left.\begin{aligned} \bar{u}_{ri} &= -\bar{F}(\omega)\omega^2 \int_0^\infty \frac{u^2}{jq_1} J_1(u\omega r)\{A_i e^{-j\omega q_i(z-z_i)} + B_i e^{+j\omega q_i(z-z_i)}\}\, du \\ \bar{u}_{zi} &= -\bar{F}(\omega)\omega^2 \int_0^\infty \frac{uq_i}{q_1} J_0(u\omega r)\{A_i e^{-j\omega q_i(z-z_i)} - B_i e^{+j\omega q_i(z-z_i)}\}\, du \end{aligned}\right\}$$
$$(i = 1, 2, \ldots, n). \tag{A-18}$$

We add a few brief remarks on some aspects of the numerical calculation of the integrals in (A-18):

1) The integration is performed by the trapezoidal rule and is restricted to the slowness interval of interest. Normally this is the interval from 0 to $1/\alpha_1$. The number of slownesses is typically 100 to several hundreds. A cosine taper at the largest slownesses may be useful to reduce the amplitudes of numerical arrivals without physical significance.

2) Anelasticity of the layers is taken into account by working with complex wave velocities according to Eq. (11) of the main paper. Besides the fact that this is a desirable feature in principle, especially when the high-frequency waves of seismic prospecting are modelled, it is also computationally favorable since it removes the surface-waves poles of the integrands away from the real u-axis and thus away from the integration path.

3) Time-domain aliasing because of very long physical responses can be avoided or reduced by using complex instead of real frequencies, as described in the main part.

4) The Bessel functions are replaced by the asymptotic form of the corresponding Hankel functions of the second kind, implying only waves propagating away from the source. Numerical tests showed that only for very accurate calculations at small distances should the original Bessel functions be retained. This may be connected with the occurrence of relatively strong numerical arrivals.

5) Fast Fourier Transform methods are used for going from the time domain to the frequency domain and vice versa.

Additional information on the numerical calculation of integrals of the form (A-18) can be found in papers by Fuchs and Müller (1971), Fertig and Müller (1978) and Kennett (1979; 1980). We conclude this appendix with the displacement spectra for a *vertical single force at the surface* of the layered medium:

$$\left.\begin{aligned} \bar{u}_{ri} &= -\frac{\bar{K}(\omega)\omega}{4\pi\rho_1} \int_0^\infty u^2 J_1(u\omega r)\{A_i e^{-j\omega q_i(z-z_i)} + B_i e^{+j\omega q_i(z-z_i)}\}\, du \\ \bar{u}_{zi} &= -\frac{\bar{K}(\omega)\omega}{4\pi\rho_1} \int_0^\infty juq_i J_0(u\omega r)\{A_i e^{-j\omega q_i(z-z_i)} - B_i e^{+j\omega q_i(z-z_i)}\}\, du \end{aligned}\right\}$$
$$(i = 1, 2, \ldots, n), \tag{A-19}$$

where

$\bar{K}(\omega) =$ force spectrum,

$$A_1 = \frac{2}{1+R}, \quad B_1 = RA_1,$$

$$A_i = 2\frac{M_{i11} + RM_{i12}}{1+R},$$

$$B_i = 2\frac{M_{i21} + RM_{i22}}{1+R} \quad (i = 2, 3, \ldots, n).$$

Formulas (A-19) are a useful supplement to the results (A-18) for an explosive point source, since these vanish for a source location at the surface because of exact cancellation of the direct wave and the surface reflection.

References

Bouchon, M.: Discrete wavenumber representation of elastic wave fields in three space dimensions. J. Geophys. Res. **84**, 3609–3614, 1979

Brekhovskikh, L.M.: Waves in layered media. New York: Academic Press 1960

Fertig, J., Müller, G.: Computations of synthetic seismograms for coal seams with the reflectivity method. Geophys. Prospecting **26**, 868–883, 1978

Fuchs, K., Müller, G.: Computations of synthetic seismograms with the reflectivity method and comparison with observations. Geophys. J. R. Astron. Soc. **23**, 417–433, 1971

Ganley, D.C.: A method for calculating synthetic seismograms which include the effects of absorption and noise. Geophysics **46**, 1100–1107, 1981

Kennett, B.L.N.: Theoretical reflection seismograms for elastic media. Geophys. Prospecting **27**, 301–321, 1979

Kennett, B.L.N.: Seismic waves in a stratified medium II – theoretical seismograms. Geophys. J. R. Astron. Soc. **61**, 1–10, 1980

Kennett, P., Ireson, R.L., Conn, P.J.: Vertical seismic profiles: Their application in exploration geophysics. Geophys. Prospecting **28**, 676–699, 1980

Müller, G.: Direct inversion of seismic observations. Z. Geophys. **37**, 225–235, 1971

O'Neill, M.E., Hill, D.P.: Causal absorption: its effect on synthetic seismograms computed by the reflectivity method. Bull. Seismol. Soc. Am. **69**, 17–25, 1979

Rosenbaum, J.M.: Synthetic microseisms: logging in porous formations. Geophysics **39**, 14–32, 1974

Wuenschel, P.C.: The vertical array in reflection seismology – some experimental results. Geophysics **41**, 219–232, 1976

Wyatt, K.D.: Synthetic vertical seismic profiles. Geophysics **46**, 880–891, 1981

Received September 23, 1981; Revised version December 17, 1981
Accepted December 17, 1981